7-2020

Synthesis And Characterization Of 3D-Printed Functionally Graded Porous Titanium Alloy

Ahmed Hindy
Shahid Beheshti University of Medical Sciences

Farzam Farahmand
Sharif University of Technology

Fereydoun Pourdanesh
Sharif University of Technology

Maryam Torshabi
Sharif University of Technology

A. Hadi Al Janabi
University of Baghdad

See next page for additional authors

Journal of Materials Science, Vol. 55, No. 21 (July 2020): 9082-9094. DOI.

Synthesis And Characterization Of 3D-Printed Functionally Graded Porous Titanium Alloy

Ahmed Hindy
Dental Research Center, Research Institute of Dental Sciences, School of Dentistry, Shahid Beheshti University of Medical Sciences, Tehran, Iran
Institute of Laser for Postgraduate Studies, University of Baghdad, Baghdad, Iraq
Farzam Farahmand
Department of Mechanical Engineering, Sharif University of Technology, Tehran, Iran
Fereydoun Pourdanesh
Department of Oral and Maxillofacial Surgery, School of Dentistry, Shahid Beheshti University of Medical Sciences, Tehran, Iran
Maryam Torshabi
Department of Dental Biomaterials, School of Dentistry, Shahid Beheshti University of Medical Sciences, Tehran, Iran
A. Hadi Al Janabi
Institute of Laser for Postgraduate Studies, University of Baghdad, Baghdad, Iraq
Morteza Rasoulianboroujeni
Marquette University School of Dentistry, Milwaukee, WI
Lobat Tayebi
Marquette University School of Dentistry, Milwaukee, WI

Fahimeh S. Tabatabaei
Dental Research Center, Research Institute of Dental Sciences, School of Dentistry, Shahid Beheshti University of Medical Sciences, Tehran, Iran
Department of Dental Biomaterials, School of Dentistry, Shahid Beheshti University of Medical Sciences, Tehran, Iran
Marquette University School of Dentistry, Milwaukee, WI

Abstract

This study aims to 3D print titanium alloy constructs incorporating gradient of porosities, from the fully dense core to the porous outer surface. Gradient porous specimens were prepared using selective laser melting (SLM). Fully dense specimens fabricated by SLM were used as the control group. Characterization of samples was done using X-ray tomography, uniaxial compression testing, and optical and scanning electron microscopes. The biocompatibility of fabricated samples was investigated using human periodontal ligament stem cells via assessment of cell attachment, viability, and proliferation by direct and indirect assays. The data were analyzed using ANOVA and Tukey’s post hoc test. Characterization of constructs reveals interconnected gradient porosities and higher contact angle in porous samples. The introduction of porosity leads to a significant decrease in compression strength. However, Young’s modulus of the samples with gradient porosity was more similar to the natural bone modulus. The surface microstructure consists of loosely bonded spherical particles. Biocompatibility of the dense and porous samples is appropriate. Although the porosity size led to a reduced cell proliferation rate in the gradient sample, the extract of the gradient sample results in more cell proliferation than the dense sample’s extract. The study demonstrates that a biocompatible functionally graded porous titanium structure can be well fabricated by SLM, and this structure leads to a good match of Young’s modulus to that of the bone.

Introduction

This study aims to 3D print titanium alloy constructs incorporating gradient of porosities, from the fully dense core to the porous outer surface. Gradient porous specimens were prepared using selective laser melting (SLM). Fully dense specimens fabricated by SLM were used as the control group. Characterization of samples was done using X-ray tomography, uniaxial compression testing, and optical and scanning electron microscopes. The biocompatibility of fabricated samples was investigated using human periodontal ligament stem cells via assessment of cell attachment, viability, and proliferation by direct and indirect assays. The data were analyzed using ANOVA and Tukey's post hoc test. Characterization of constructs reveals interconnected gradient porosities and higher contact angle in porous samples. The introduction of porosity leads to a significant decrease in compression strength. However, Young's modulus of the samples with gradient porosity was more similar to the natural bone modulus. The surface microstructure consists of loosely bonded spherical particles. Biocompatibility of the dense and porous samples is appropriate. Although the porosity size led to a reduced cell proliferation rate in the gradient sample, the extract of the gradient sample results in more cell proliferation than the dense sample's extract. The study demonstrates that a biocompatible functionally graded porous titanium structure can be well fabricated by SLM, and this structure leads to a good match of Young's modulus to that of the bone.

Increasing applications of implantable biomaterials in orthopedics and dentistry lead to the rapid development of new technologies in this field. The purpose of these new technologies is to enhance both physical and biological responses of bed tissue, promote osseointegration, reduce treatment time, and increase success rate and survival rate of implants. The strength, stiffness, and abrasion resistance are the most important properties in the orthopedic implant—as artificial bone. On the other hand, the small size of a dental implant—as artificial tooth root—and the special way of its placement in the jawbone, make stress relaxation more important for the part inside of the bone, and require sufficient strength for the part in contact with the oral cavity [[1]]. However, the primary objective of any implant system is to have a firm fixation to the bone, and this objective could be influenced by biomechanical and biomaterial selection [[2]]. Bone-implant modulus mismatch, as well as the inadequate initial fixation with the host bony tissue, are the two severe problems that researchers are currently dealing with [[4]]. Bone tissue surrounding the implant is subject to some mechanical stress. Insufficient loading following the mismatch of Young's module is termed stress shielding, which may detrimentally affect the bone and lead to resorption [[5]].

Although titanium and its alloys have considerable advantages—like excellent biocompatibility—there are also certain drawbacks, like its elastic modulus (110–120 GPa), which is far higher than that of cortical bone (10–30 GPa). The introduction of porosity into the structure of titanium and its alloys can reduce the elastic modulus of Ti so that it more closely matches the human bone. It brings also other benefits, like lowering the density of implants and improving tissue adhesion [[7]]. Trabecular Metal™ (Zimmer, Warsaw, IN, USA), a highly porous carbon matrix coated with tantalum (Ta), is one of the commercialized porous metal bone replacement structures [[9]]. Following a biomimetic approach, a gradient in porosity as seen in natural bone could also be applied in the manufacturing of orthopedic and dental implants. Replication of this functional gradient ensures the right distribution of compressive stiffness across various regions. However, the creation of functionally graded structures cannot be accomplished with a conventional machining technique, assuming the need for evolving technologies. Three-dimensional printing (3DP) or additive manufacturing (AM) can generate objects with defined structure and shape based on three-dimensional (3D) data. These technologies could manufacture implants with both porous and solid sections in one step and provide good control over the pore size, shape, and distribution [[10]]. One of the processing techniques for AM technologies is selective laser melting (SLM) [[12]]. In SLM, after designing the gradient structure, the scan of the powder with a laser beam would result in a porous structure. The porosity is under the control of laser spot diameter and particle size and morphology of powder [[14]].

Understanding the structure–property relationship of porous metals has a huge impact on the progress of orthopedic and dental implants. Although manufacturing of porous titanium alloy based on SLM process is the focus of several research groups, the great versatility of the process and different parameters used to create these materials leaves many potential designs unexplored [[15]]. Furthermore, the dental implant is replacing the tooth root, and the assessment of the interaction of the periodontal ligament stem cells (PDLSCs) is very important in relation to the surface of the designed implant. This article discusses the feasibility of fabrication of titanium specimens by SLM method and determines the effect of gradient porosities (with two different strut diameters) on the physical and biological properties in comparison with fully dense structures.

Materials and methods

3D printing of samples

A spherical Ti–6Al–4V powder (EOS München, Germany, 5–50 µm) was selected as our starting material. Processing was carried out under the vacuum with an argon atmosphere using 400 W Yb-fiber (1034 nm) laser system (EOS M 290 GmbH Munchen, Germany). Laser processing parameters were set up as indicated in Table 1.

Table 1. Laser processing parameters

Laser	**400 W Yb-fiber (1034 nm)**
Scanning rate	7 m/s
Laser spot diameter	82 µm
Laser power	175 W
Scan speed	2000 mm/s
Beam compensation	0.139 mm
Layer thickness	30 µm

To study the influence of gradient porosity, a fully dense sample was printed as control group. Two gradient lattice structures with a dense core and a surrounding porous lattice structure were designed using 3-matic software (Materialize, Leuven, Belgium) and 3D printed. Gradient 1 (G1) was created with struts diameter varying from 340 µm to 250 µm, and Gradient 2 (G2) with struts diameter from 380 µm to 200 µm. Strut diameter was reduced from the dense core toward the outer surface. Figure 1 shows the cubic samples designed with dimensions of 8 × 8 × 8 mm and dodecahedron unit cell, with possible applications as dental or orthopedic implants.

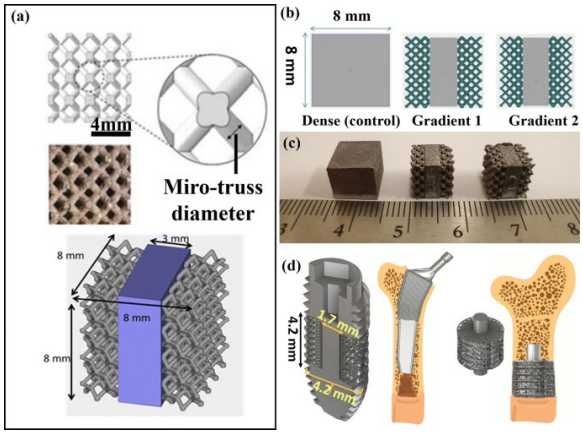

Figure 1 Different views of samples. a 3D CAD visual representation of unit-cell structure (top) of the gradient porous specimen and top and isometric view, b section view of software models, c macroscopic images showing the front view of manufactured specimens intended for characterization: fully dense, gradient-1, and gradient-2, d schematic illustration representing the possible applications of the designed construct as dental or orthopedic implants

Finally, the prepared samples were subjected to heat treatment in an argon atmosphere at 600 °C for 3 h. Samples were then cut off from the base plate. After finishing, the samples were sonicated for 10 min in acetone at 25 °C to remove residual particles from the manufacturing process.

Characterization

The porosity of the 3D-printed porous samples was calculated by comparing the bulk density of samples that is the ratio of weight/volume with the theoretical density of Ti6Al4V, which is 4.45 g/cm^3. Relative density was calculated as follow:

$$\text{Relativedensity} = 1 - (\text{Poresvolume}/\text{Totalvolume}).$$

Surface wettability of samples was assessed with contact angle measurements. The contact angle was measured by deposition of 5 µl drops of distilled water on three locations per sample and videos acquisition of these drops.

To evaluate the graded lattice structure, X-ray tomography was performed using X-ray computer tomography (CT, YXLON International X-ray GmBH, Germany). A source voltage of 180 kV and a detector size of 1024 × 1024-pixel were selected as the scanning parameters. A total of 1620 projections were recorded and reconstructed by employing the filtered back-projection procedure.

Mechanical properties of SLM processed samples were determined using the compression test in the longitudinal and transverse directions. Five samples (*n* = 5) for each of the three different groups were tested using a universal testing machine (MTS System Corporation, Saint-Etienne, France) with a 250 kN load cell. The machine was equipped with an MTS extensometer to measure strain. A commercial 3D digital image correlation (DIC) system was also used to analyze the samples displacement during the compression test. The samples were prepared for DIC by applying a random black-on-white speckle pattern to the specimen surface using aerosol spray painting. The optical system was equipped with two high-resolution cameras (5 Million pixels) coupled with two lenses. The analysis based on the pairs of images recorded during the object deformation was performed using the photogrammetric software program (Aramis, GOM GmbH, Germany). Figure 3a shows the graphs of the longitudinal and transversal loading of samples and the method of photogrammetry.

The scanning electron microscope (SEM; Seron Technology-AIS-2300C, Korea) operating at 20 kV was used to observe the surface morphology of the SLM-fabricated samples and the fracture surfaces after compression test. Samples surface morphologies were also observed by an optical microscope (Evos Fl, life technologies).

Biocompatibility assessment

Normal human third molars extracted from two healthy adults undergoing tooth extraction were used for isolation of periodontal ligament stem cells (PDLSCs) under approved guidelines set by the Institutional Review Board of Marquette University (Milwaukee, USA). PDL tissues were gently scraped from the middle third of the root surface by using a scalpel, then minced and digested in a solution of 3 mg/mL collagenase type I (Sigma Chemical, St. Louis, MO, USA) and 4 mg/ml of dispase (Sigma-Aldrich, St. Louis, MO, USA) for 1.5 h in an incubator. Cells were transferred into a small flask and incubated in the Dulbecco's modified Eagle's medium (DMEM) (Corning, Mediatech Inc., USA) supplemented with 10% v/v fetal bovine serum (FBS, Sigma, USA) for 7 days. The cultures were kept in an incubator at 37 °C and 5% CO_2 until the fourth passage was reached. For flow cytometric analysis, fresh cell suspensions (10^6 cells/ml) were washed in blocking buffer (containing 3% bovine serum albumin) and incubated for 45 min at 4 °C in the dark with an appropriate amount of the following antibodies: FITC conjugated anti-CD90 (0.5 mg/ml) or FITC Mouse IgG1 Control, FITC anti-human CD44 (200 µl/ml) or

FITC-conjugated mouse IgG2b control, phycoerythrin (PE) anti-human CD34 (200 µl/ml), and PE anti-human CD45 (200 µl/ml) or PE-conjugated mouse IgG1 control. Finally, the expression profiles were analyzed using the attune acoustic focusing cytometer (Applied Biosystems, USA).

The multipotency of PDLSCs was investigated by testing the ability of isolated cells to undergo osteogenic and adipogenic differentiation. To detect osteogenic differentiation, Alizarin Red staining (EMD Millipore, USA) was used 21 days after seeding of cells (1×10^4 cells/well of 6-well plates) in osteogenic media (DMEM supplemented with 100 nM dexamethasone, 0.05 M ascorbate-2-phosphate, 10 mM β-glycerophosphate, 1% antibiotic/antimycotic (Sigma, USA) and 10% FBS). Adipogenesis was assessed 21 days after seeding of cells (2×10^4 cells/well) in adipogenic media (DMEM supplemented with 10% FBS, 0.5 mM isobutyl-methyl-xanthine, 1 mM dexamethasone, 10 µg/ml insulin, 100 M indomethacin and 1% antibiotic/antimycotic) with Oil red O (Sigma Chemical) staining.

Specimens were sterilized by gamma radiation at 25–45 kGy doses and placed in the 24-well plate (SPL, Korea). Biocompatibility studies were performed by using direct and indirect assays. For direct contact assessment, the fourth passage hPDLSCs (1×10^5 cells/sample) were drop seeded directly on the constructs. The cells were allowed to attach to the samples for 2 h at 37 °C. The samples were then transferred to a new plate, immersed in a regular culture medium (DMEM supplemented with 10% FBS and 1% antibiotic–antimycotic) and incubated at 37 °C in 5% CO_2. After 24- or 72-h incubation, cellular metabolic activity was assessed by exchanging the medium of each well with 3-(4,5-dimethylthiazol-2-yl)-2,5-diphenyltetrazolium bromide (MTT) (0/5 mg/mL; Sigma-Aldrich, Germany), following by 2 h incubation at 37 °C. The MTT medium was then replaced with dimethyl sulfoxide solvent, and 100 µl of the colored solution from each group was added to each well of a 96-well plate. The optical density (OD) was read at 570 nm (main) and 620 nm (reference) wavelengths by a microplate reader (Anthos 2020, Austria). The percentage of cell viability was obtained as the ratio of the gradient samples' OD value to the mean of control groups' OD value. PrestoBlue® assay (Invitrogen) was also performed to measure cell proliferation at 2 and 7 days after cell seeding on gradient and dense samples. Briefly, a 10% v/v solution of PrestoBlue in phenol red-free DMEM was added to the seeded samples at the appropriate time point and incubated at 37 °C in 5% CO_2 for 1 h. The fluorescence was measured at excitation/emission wavelengths of 540/590 nm using a microplate reader (Biotek Instruments, Inc., Vermont, USA).

For a qualitative evaluation of cells seeded on the samples, the LIVE/DEAD® viability assay was performed. The medium was removed 24 h after incubation of seeded samples, and the samples were rinsed and treated with 5 µM Calcein-AM, and 4 µM ethidium homodimer-1 (LIVE/DEAD, Life Technologies, California, USA) in 1 × Dulbecco's phosphate buffered saline (D-PBS, Life Technologies) for 10 min. Z-stacks images were obtained using an Olympus microscope (Evos Fluorescent, Life Technologies).

Cell attachment on samples was assessed 24 h after seeding using SEM. The hPDLSCs-seeded constructs (1×10^5 cells/specimen) were rinsed with PBS and fixed in 2.5% glutaraldehyde (Merck, Darmstadt, Germany). The samples were dehydrated in graded concentrations of ethanol (from 30 to 100% v/v in distilled water), then gold-coated and observed under a scanning electron microscope (AIS-2300C-SEM, Seron Technology, Korea).

For the indirect assay, the extract media of samples was prepared by incubating sterilized gradient-2 and dense samples in culture media (without FBS) at a concentration of 1.25 cm^2/ml at 37 °C (according to ISO 10993). After 48 h, the extract media was filtered and supplemented with 10% FBS and 1% antibiotic–antimycotic. The extract media was used for the treatment of PDLSCs seeded in a 96-well plate at a density of 3000 cells/well. After 7 days, cell viability was assessed using the CellTiter-Glo (Promega, Madison, WI). Briefly, the media was removed, 50 µl of PBS was mixed with 50 µl ATP assay reagent and added to each well. The plate was incubated at room temperature for 10 min, and then, luminescence was recorded in a microplate reader (Biotek Instruments, Inc., Vermont, USA).

Statistical analysis

The data were analyzed by one-way ANOVA and post hoc Tukey's test using GraphPad Prism (V.6.07) (GraphPad Software, Inc, La Jolla, USA). A *p* value of less than 0.05 was considered significant.

Results

Characterization

3D-printed gradient constructs have 49.195% (G1) and 48.720% (G2) theoretical porosity, respectively (Table 2). The contact angle of the control group (71.17 ± 4.82°) is significantly lower than the gradient samples (~ 100°), and there is no significant difference between G1 and G2 (Fig. 2c).

Table 2. Theoretical calculations of the porosity in the specimens and their contact angle

	Bulk vol. (mm^3)	**Pores vol. (mm^3)**	**Pores (%)**	**Weight (g)**	**Density (g/cm^3)**	**Relative density**	**Contact angle (degree)**
D	512.00	00	0	2.28	4.4531	1	71.17 ± 4.82
G1	260.124	251.876	49.195	1.27 ± 0.012	2.4804	0.508	102.63 ± 3.79
G2	262.552	249.448	48.720	1.28 ± 0.005	2.5000	0.513	100.095 ± 9.1

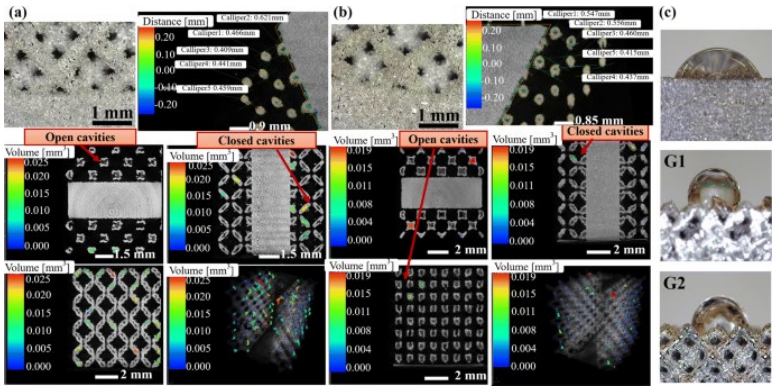

Figure 2 Digital micrograph of SLM specimen surface (top right corner) and x-ray tomography cross sections of laser sintered 3D samples showing the thickness of the strut diameter from the central part toward the ends in G1 (a) and G2 (b). The contact angle of dense and gradient samples (c)

Using X-ray tomography to evaluate the graded lattice structure shows a different diameter in the thickness of the struts in comparison with the original designed structure. Theoretical strut diameter

(from designed files) varied from 340 to 250 µm for G1, and from 370 to 200 µm for G2. Figure 2a, b shows different struts diameters measured from 621 to 459 µm (a) and 556 to 415 µm (b), which are bigger than expected because of the collapse of the lattices' down-skin. The open- and closed-pores can be identified in different section views of gradient samples.

Static compression test was accompanied by DIC using the ARAMIS software, as virtual extensometer, to evaluate specimen deformation during test (Fig. 3a). Dense sample shows higher strength and stiffness than gradient samples. However, there are no significant differences between mechanical properties of gradient samples ($p > 0.05$) (Fig. 3b, c). Compressive strength and elastic modulus are higher in the longitudinal than in the transversal direction in both gradient samples ($p < 0.05$). Digital recording of compressive response by DIC shows the formation of crush bands during deformation, with an angle of about 45º in gradient samples.

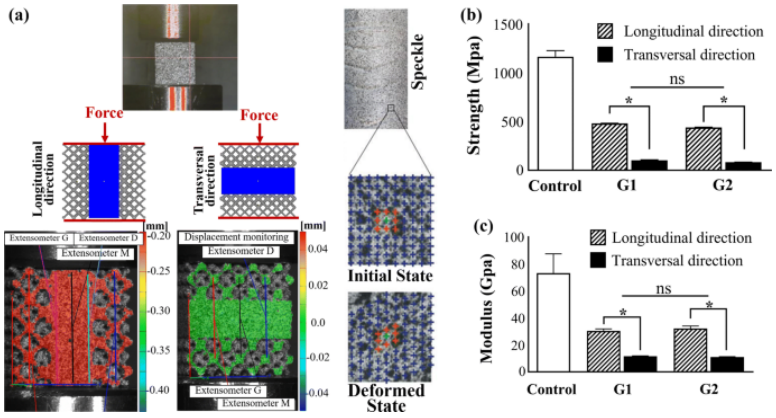

Figure 3 Representation of mechanical properties measurement in longitudinal and transversal direction and DIC pictures (a). Compressive strength (b) and Young's modulus of elasticity (c) of dense and porous specimens. Stars (*) on the columns (gradient samples) indicate statistically significant differences with the non-gradient control group (*p < 0.05). ns: non-significant

Loosely bound unmelted spherical particles are evident on the surface of the control group and gradient samples under SEM. The size of these particles is in the range of 5–46 µm (Fig. 4a, b). Figure 4c, d shows the fracture surfaces of the samples following the compression test. The full dense specimen (control group) expresses high strength against compression force.

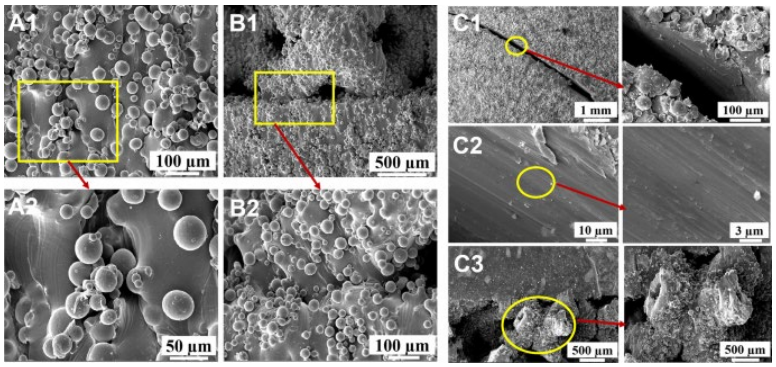

Figure 4 SEM images showing the surface morphology of SLM-fabricated samples before and after the fracture. A1 and A2 control group (dense sample) surface: High magnification image in A2 shows the size of loosely bound particles after production; B1 and B2 gradient sample; C1 and C2 fracture

surfaces of the dense sample subjected to a static compression force; C3 the fracture surface of the gradient porous specimen

Biocompatibility

In this study, we used PDLSCs to assess the biocompatibility of our samples. Flow cytometry and multipotent capability of cells confirm their stemness property. The PDLSCs are positive for mesenchymal stem cells-related antigen CD90, CD44, and CD105, while being negative for the hematopoietic cell antigens CD34 and CD45. The expression level of surface markers is represented in Table 3. Differentiation into osteoblasts and adipocytes is also confirmed after 4 weeks of cell culturing in osteogenic and adipogenic media, by Alizarin red and Oil red O staining (Fig. 5).

Table 3. The expression levels of surface markers by PDLSCs (%)

	CD90	**CD44**	**CD105**	**CD34**	**CD45**
PDLSCs	99.98	97.78	96.08	0.92	0.64

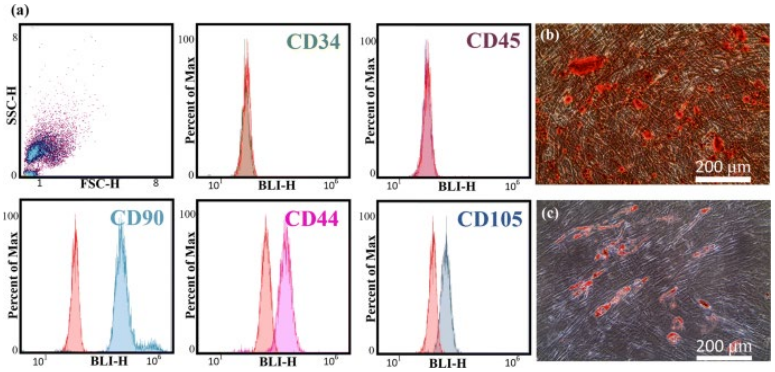

Figure 5 Flow cytometry data and images of multipotent differentiation of PDLSCs. a Expression of negative markers (CD34 and CD45) and positive markers (CD90, CD44, and CD105) in comparison with IgG controls (isotype control are marked with red solid histogram). b positive staining of mineralized nodules after 3 weeks of osteogenic induction confirmed by Alizarin Red staining. c positively stained lipid vacuoles after 3 weeks of adipogenic induction as confirmed by Oil Red O staining

The proliferation of hPDLSCs seeded on the SLM titanium alloy constructs is evaluated using MTT assay at 24 and 72 h after exposure. As seen in Fig. 6a, the lower cell viability percentage after 24 h seeding on gradient groups (35.3 ± 6.1% and 29 ± 3.9% for the gradient-1 and gradient-2, respectively), compared to the dense group (control group, 100% viability) indicates lower initial cell attachment. According to the MTT results, a significant time-dependent increase in viability is seen in both gradient groups: 59.3 ± 10.5% for the gradient-1 and 50.6 ± 9.2% for gradient-2. No significant difference in cell viability is seen in the gradient-1 compared to gradient-2 at 24 and 72 h. The results of the PrestoBlue assay confirm the abovementioned results of MTT (Fig. 6b). There is significantly more cell proliferation on the dense sample in both time points ($p < 0.05$). However, cell treatment with the extract of samples shows an opposite effect. The cell cytotoxicity due to chemicals leached from the dense and gradient samples obtained from the indirect study (CellTiter-Glo assay) is shown in Fig. 6c. It can be observed that PDLSCs treated with the extract of the dense sample have significantly lower cell proliferation than those treated with the extract of the gradient sample ($p < 0.05$).

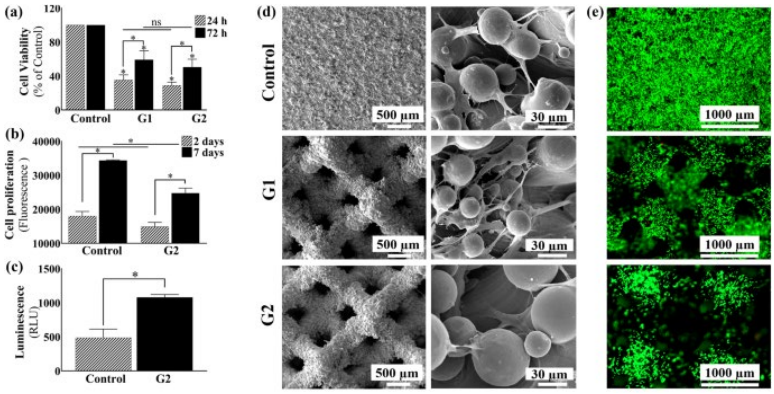

Figure 6 Cell response to laser-sintered surfaces by direct and indirect studies. a Results of the MTT assay after 24 and 72 h culture of hPDLSCs on three different groups of SLM titanium alloy constructs: dense (control), gradient-1, and gradient-2. b Results of PrestoBlue assay after 2- and 7-days cultures of hPDLSCs on dense, and gradient-2 samples. c Results of the CellTiter-Glo luminescent cell viability assay after 7 days culture of hPDLSCs treated with the extract of dense and gradient-2 specimens. d The SEM micrographs showing cell attachment of hPDLSCs after 24 h culture on dense, gradient-1 and gradient-2 titanium specimens. e Cell viability (live = green, dead = red) after culturing PDLSCs until confluence on samples. * = $p < 0.05$, G1: Gradient 1, G2: Gradient 2, ns: non-significant

The cell attachment and morphology are investigated by SEM (Fig. 6d). The SEM images show thin projections extending from the hPDLSCs (filopodia), which is a sign of good attachment to our SLM constructs. The cell-to-cell and cell-to-surface connections are clearly observable. Also, the result of live/dead staining shows a good attachment of cells on the constructs. As seen in Fig. 6e, the morphology of attached cells is normal with few apoptotic cells.

Discussion

Design

In this study, we confirmed the feasibility of manufacturing functionally graded porous titanium implants by using SLM. The powder material, particle size, and processing parameters of printing are very important for the design of functionally graded materials. Despite the relatively high stiffness of titanium to that of the bone, it is still considered to be the material of choice in orthopedic and dental implant fabrication, due to its proper biocompatibility and mechanical properties [[17]]. In our study, we preferred using one of the titanium alloys since it is the alloy of choice for any sort of situation where a combination of high strength, lightweight, good corrosion resistance, and high toughness are required. The size of the metal powder used in 3D printing influences the apparent density, essential energy input for powder melting, powder leveling fluidity, reaction with oxygen, and surface accuracy of forming samples. Particle size smaller than 5 µm is not recommended because of the possible danger to experimental personnel and potential pollution. Usually, a mixture of different sizes of powder distributed in a certain range is used. In this study, a particle size of 5–50 µm was employed due to its suitability for SLM method [[19]]. In the design of our gradient samples, we used high stiff core for bearing the load, and porous exterior layers for reducing the overall stiffness of the implants. The approximation of the elastic modulus of the implant and bone would enhance the osseointegration [[20]]. We succeeded in the construction of the open interconnected gradient porous

lattice with a dense core and a porosity of about 50%. Van Grunsven et al. [[22]] also designed and processed a Ti6Al4V sample of a regular diamond lattice incorporating graded porosity. However, their method of fabrication was electron beam melting (EBM). We used SLM, as this method can offer well defined and controlled geometry—like 3D open lattice structure [[23]]—and allow for the manufacturing of 3D porous titanium constructs of precise micro-architecture design [[24]].

In our study, the unit cell of gradient samples was dodecahedron, as used by Ahmadi and Fousová [[15], [25]]. The design of the unit cell and porous structure has a great impact on the functionality of constructs. Several designing ways of porous structures had introduced by Parthasarathy et al. [[26]] and Lin and Wirtz [[27]]. These porous structures produced by SLM were used as important reference in our experiment.

Characterization

Morphological analysis using X-ray computed tomography revealed the regular dodecahedral architecture of the porous structure with a highly repeatable overall porosity due to controlled fabrication. Kim et al. [[28]] in their study used X-ray microtomography (μCT) to validate structural properties of the SLM produced porous titanium samples with 60 and 75% porosity levels. Our data showed different struts diameters of printed samples in comparison with designed files. Kerckhofs et al. [[29]] and Van Bael et al. [[30]], who used μCT to evaluate the SLM-builted porous Ti constructs, also reported the possibility of difference between the original design and final products. One possible explanation of this difference is the beam compensation used to fuse lattice structure. The second explanation of differences is the collapse of the down-skin of the lattice. This type of defect is common in the laser beam melting technology.

Our data demonstrate a good match of Young's modulus in the gradient samples to that of the bone. Yavari et al. [[24]] also fabricated porous structures of dodecahedron designed micro-architecture, using spherical pre-alloyed Ti6Al4V ELI powder and SLM method and reported mechanical properties in the range of the bone. In our samples, the measured values for Young's modulus range between 29.20 ± 6.27 and 26.96 ± 2.02 Gpa for porous samples, which is similar to the result of Fousová et al. [[15]] who produced three types of gradient porous specimens of Ti6Al4V (30.5 ± 2 GPa). Lin et al. [[31]] also demonstrated a Young's modulus of 35 GPa in the gradient titanium constructs with a laser-sintered porous core and a solid skin. However, in the study of Traini et al., who produced gradient porous titanium alloys using the particle size of 1–10 μm via direct laser metal sintering, Young's modulus of porous samples (77 ± 3.5 GPa) was slightly more than that of the bone (20 ± 7.0 GPa) [[32]]. Although the strength of our gradient samples (75–102 MPa) was less than the fully dense control group, this reduction is absolutely logic in the porous structures. Introduction of 50% porosity in the structure could reduce the strength by 57–60% [[15]]. Parthasarathy et al. [[26]] also proved that modification of the strut thickness of the 3D-printed samples could cause strength reduction. This could be optimized by changing the shape or topology of pores, or other geometric parameters in future studies [[33]]. DIC simulation did not show yielding at the interfaces between layers, which was in agreement with the study of Zhang et al. [[34]] on functionally graded porous Ti–6Al–4V.

Bone affinity and stress relaxation are more important for the part of the dental implant inside the jawbone, while more strength is required for the part near the oral cavity. Taking these points into account, the best possible design for a standard dental implant with 4.2 mm diameter and 10.0 mm

length is proposed in Fig. 1d. The size of the solid core in our samples was 3 mm, and the porous part had a thickness of 2.5 mm which should be reduced to 1.7 mm and 1.25 mm, respectively, for the proposed dental implant. Increasing the ratio of the solid core to the thickness of the gradient porous part from 1.2 to 1.36 mm for a reliable dental implant construct would probably improve the mechanical properties. Properties such as strength and stiffness are more important in orthopedic implants than dental implants; therefore, designing orthopedic implants requires more reduction in the thickness of the porous part. Possible applications in orthopedics are shown in Fig. 1d.

Surface morphology and contact angle are important features in defining the interaction of cells with a surface [[35]]. The contact angle of our gradient samples was greater than the control group, which indicates they are not ideal for allowing the first attachment of cells. The surface of our samples also showed loosely bound or partially sintered particles, which is inevitable in SLM based on the report of Vaithilingam et al. [[16]], who fabricated TI6Al4V constructs by SLM and inspected the surface chemistry. However, it should be noted that the magnitude of this problem (the presence of partially melted particles on the surface) is dependent on both material and processing parameters [[36]]. In order to prevent the interference of these loosely bound Ti particles with bone formation, removing them with different techniques is essential [[31]]. In the SEM fractography, the coalescence of microvoids approved ductile fractures of all samples. This finding is clearly similar to those of Traini et al. [[31]], who examined the fractured surface. Ductility of SLM samples can be increased by applying heat treatments after laser melting fabrication [[38]].

Biocompatibility

Since the periodontal ligament supports tooth root, and dental implants are supposed to substitute the root of missing teeth, we considered hPDLSCs for evaluating the interaction of cells in relation to the surface of the designed samples. PDLSCs can differentiate into different cell lines and show different performances depending on the surface where they are seeded [[39]]. Other studies used human osteoblasts or human dental pulp stem cells (DPSCs) for biocompatibility assessment of implants [[40]]. Cell attachment and cell proliferation are the most current in vitro assays used for inspecting the biological outcome of dental implants [[42]]. Based on our data, hPDLSCs were attached well, and SLM fabricated titanium constructs demonstrated no cytotoxic effect. Healthy cells morphology, which was confirmed by SEM, and the low number of red cells in the live/dead assay confirmed non-toxicity of our samples. In our study, assessment of cell proliferation on the samples was done by direct and indirect assays via MTT, PrestoBlue and CellTiter-Glu assay. In direct studies, gradient samples showed lower cell proliferation than the flat surface of the control group. The size of porosities in these samples could explain these results. A study by De Peppo et al. [[43]] shows that surface morphology of EBM-fabricated cpTi, and Ti6Al4V porous scaffolds could affect cell attachment and proliferation of embryonic stem cells. However, it could be possible to see a different behavior in vivo, as indicated by Karageorgiou and Kaplan [[44]]. They found that lower porosity is preferable in vitro, as there is no flow of culture media; however, in vivo, larger bone ingrowth is the result of higher porosity and pore size. Although dense sample can provide more initial cell attachment, easier cell infiltration provided by larger pores was shown to be more important and may also facilitate angiogenesis throughout gradient structure [[45]]. Improved cell distribution within the gradient scaffolds in comparison with the non-gradient samples was shown in the study of Sobral et al. [[46]]. Furthermore, gradient configurations in the porosity of the samples have many advantages over the non-gradient ones in

terms of cell migration, nutrient delivery, and gas diffusion. Possible cell polarization and a gradient in oxygen tension in response to gradient configuration can explain gradient-dominated cell migration and differentiation [[47]].

Results of our indirect study, which assess the cytotoxicity as a result of chemical leaching, showed an opposite effect in comparison with the direct study. The CellTiter-Glu assay showed more cell proliferation under treatment with extract of the gradient sample than the control group. One possible explanation of this result could be a greater release of loosely bound particles from the surface of the control group. More work will be required to study the composition of the extract media of gradient and dense samples, differentiation potential of stem cells on the surface of SLM fabricated samples, and in vivo responses.

Conclusion

In this study, Ti–6Al–4V powder was used for fabrication of gradient porous structures via SLM process. Microstructure, mechanical properties, and biocompatibility of samples were characterized. The results revealed that SLM constructs have partially melted particles on the surface. Functionally graded samples with a dense core had a good match of Young's modulus to that of the bone. Large porosities and higher contact angle of gradient samples led to a lower initial cell attachment on their surface. However, the extract of gradient samples resulted in more cell proliferation than the dense sample's extract. There were no significant differences between the two designed lattice constructs.

Acknowledgements

This study was supported by a Grant from the Iran National Science Foundation (Project No. 95819948). The authors would like to acknowledge the efforts of Mojtaba Javid for designing proposed applications in orthopedics and dental implants.

Compliance with ethical standards

Conflict of interest

The authors declare that they have no conflict of interest.

Publisher's Note

References

1. *Watari F, Yokoyama A, Omori M, Hirai T, Kondo H, Uo M, Kawasaki T. Biocompatibility of materials and development to functionally graded implant for bio-medical application. Compos Sci Technol. 2004; 64; 6: 893-908. 10.1016/j.compscitech.2003.09.005*
2. *Ahuja A, Ahuja V, Singh K. Current concepts of regenerative biomaterials in implant dentistry. J Int Clin Dent Res Organ. 2015; 7; 3: 34-39. 10.4103/2231-0754.172943*
3. *Saini M, Singh Y, Arora P, Arora V, Jain K. Implant biomaterials: a comprehensive review. World J Clin Cases. 2015; 3; 1: 52-57. 10.12998/wjcc.v3.i1.52*

4. *Brunski JB. Biomaterials and biomechanics in dental implant design. Int J Oral Maxillofac Implants. 1988; 3; 2: 85-97*
5. *Deing A, Luthringer B, Laipple D, Ebel T, Willumeit R. A porous TiAl6V4 implant material for medical application. Int J Biomater. 2014; 2014: 8. 10.1155/2014/904230*
6. *Ryan G, Pandit A, Apatsidis DP. Fabrication methods of porous metals for use in orthopaedic applications. Biomaterials. 2006; 27; 13: 2651-2670. 10.1016/j.biomaterials.2005.12.002*
7. *Wally Z, van Grunsven W, Claeyssens F, Goodall R, Reilly G. Porous titanium for dental implant applications. Metals. 2015; 5; 4: 1902. 10.3390/met5041902*
8. *Kelly CN, Evans NT, Irvin CW, Chapman SC, Gall K, Safranski DL. The effect of surface topography and porosity on the tensile fatigue of 3D printed Ti–6Al–4V fabricated by selective laser melting. Mater Sci Eng C. 2019; 98: 726-736. 10.1016/j.msec.2019.01.024*
9. *Bencharit S, Byrd WC, Altarawneh S, Hosseini B, Leong A, Reside G, Morelli T, Offenbacher S. Development and applications of porous tantalum trabecular metal-enhanced titanium dental implants. Clin Implant Dent Relat Res. 2014; 16; 6: 817-826. 10.1111/cid.12059*
10. *Sing SL, Tey CF, Tan JHK, Huang S, Yeong WYNarayan R. 2–3D printing of metals in rapid prototyping of biomaterials: techniques in additive manufacturing. Rapid prototyping of biomaterials. 20202: Cambridge; Woodhead Publishing: 17-40*
11. *Zhang C, Chen F, Huang Z, Jia M, Chen G, Ye Y, Lin Y, Liu W, Chen B, Shen Q, Zhang L, Lavernia EJ. Additive manufacturing of functionally graded materials: a review. Mater Sci Eng A. 2019; 764: 138209. 10.1016/j.msea.2019.138209*
12. *Xiong Y, Qian C, Sun J. Fabrication of porous titanium implants by three-dimensional printing and sintering at different temperatures. Dent Mater J. 2012; 31; 5: 815-820. 10.4012/dmj.2012-065*
13. *Wang S, Liu L, Li K, Zhu L, Chen J, Hao Y. Pore functionally graded Ti6Al4V scaffolds for bone tissue engineering application. Mater Des. 2019; 168: 107643. 10.1016/j.matdes.2019.107643*
14. *Wang M, Wu Y, Lu S, Chen T, Zhao Y, Chen H, Tang Z. Fabrication and characterization of selective laser melting printed Ti–6Al–4V alloys subjected to heat treatment for customized implants design. Prog Nat Sci Mater. 2016; 26; 6: 671-677. 10.1016/j.pnsc.2016.12.006*
15. *Fousová M, Vojtěch D, Kubásek J, Jablonská E, Fojt J. Promising characteristics of gradient porosity Ti–6Al–4V alloy prepared by SLM process. J Mech Behav Biomed. 2017; 69; Supplement C: 368-376. 10.1016/j.jmbbm.2017.01.043*
16. *Vaithilingam J, Prina E, Goodridge RD, Hague RJM, Edmondson S, Rose FRAJ, Christie SDR. Surface chemistry of Ti6Al4V components fabricated using selective laser melting for biomedical applications. Mater Sci Eng C. 2016; 67; Supplement C: 294-303. 10.1016/j.msec.2016.05.054*
17. *Niinomi M. Mechanical biocompatibilities of titanium alloys for biomedical applications. J Mech Behav Biomed. 2008; 1; 1: 30-42. 10.1016/j.jmbbm.2007.07.001*
18. *Sidambe AT. Biocompatibility of advanced manufactured titanium implants—a review. Materials. 2014; 7; 12: 8168-8188. 10.3390/ma7128168*
19. *Zheng Y, Xu X, Xu Z, Wang J, Cai H (eds) (2017) Titanium implants based on additive manufacture. In: Metallic biomaterials: new directions and technologies, 1st edn. Wiley-VCH Verlag GmbH & Co. KGaA, pp 255–291*

20. *Chen WM, Xie Y, Imbalzano G, Shen J, Xu S, Lee S-J, Lee P. Lattice Ti structures with low rigidity but compatible mechanical strength: design of implant materials for trabecular bone. Int J Precis Eng Manuf. 2016; 17; 6: 793-799. 10.1007/s12541-016-0097-6*
21. *Nune KC, Kumar A, Misra RDK, Li SJ, Hao YL, Yang R. Functional response of osteoblasts in functionally gradient titanium alloy mesh arrays processed by 3D additive manufacturing. Colloid Surf B. 2017; 150; Supplement C: 78-88. 10.1016/j.colsurfb.2016.09.050*
22. *van Grunsven W, Hernandez-Nava E, Reilly GC, Goodall R. Fabrication and mechanical characterisation of titanium lattices with graded porosity. Metals. 2014; 4; 3: 401-409. 10.3390/met4030401*
23. *Zhang Q, Liang Z-l, Cao M, Liu Z-f, Zhang A-f, Lu B-H. Microstructure and mechanical properties of Ti6Al4V alloy prepared by selective laser melting combined with precision forging. Trans Nonferrous Met Soc. 2017; 27; 5: 1036-1042. 10.1016/S1003-6326(17)60121-3*
24. *Amin Yavari S, Wauthle R, van der Stok J, Riemslag AC, Janssen M, Mulier M, Kruth JP, Schrooten J, Weinans H, Zadpoor AA. Fatigue behavior of porous biomaterials manufactured using selective laser melting. Mater Sci Eng C. 2013; 33; 8: 4849-4858. 10.1016/j.msec.2013.08.006*
25. *Ahmadi S, Yavari S, Wauthle R, Pouran B, Schrooten J, Weinans H, Zadpoor A. Additively manufactured open-cell porous biomaterials made from six different space-filling unit cells: the mechanical and morphological properties. Materials. 2015; 8; 4: 1871-1896. 10.3390/ma8041871*
26. *Parthasarathy J, Starly B, Raman S. A design for the additive manufacture of functionally graded porous structures with tailored mechanical properties for biomedical applications. J Manuf Process. 2011; 13; 2: 160-170. 10.1016/j.jmapro.2011.01.004*
27. *Lin CY, Wirtz T, LaMarca F, Hollister SJ. Structural and mechanical evaluations of a topology optimized titanium interbody fusion cage fabricated by selective laser melting process. J Biomed Mater Res A. 2007; 83; 2: 272-279. 10.1002/jbm.a.31231*
28. *Kim TB, Yue S, Zhang Z, Jones E, Jones JR, Lee PD. Additive manufactured porous titanium structures: through-process quantification of pore and strut networks. J Mater Process Technol. 2014; 214; 11: 2706-2715. 10.1016/j.jmatprotec.2014.05.006*
29. *Van Bael S, Kerckhofs G, Moesen M, Pyka G, Schrooten J, Kruth J-P. Micro-CT-based improvement of geometrical and mechanical controllability of selective laser melted Ti6Al4V porous structures. Mater Sci Eng A. 2011; 528; 24: 7423-7431. 10.1016/j.msea.2011.06.045*
30. *Kerckhofs G, Schrooten J, Van Cleynenbreugel T, Lomov SV, Wevers M. Validation of x-ray microfocus computed tomography as an imaging tool for porous structures. Rev Sci Instrum. 2008; 79; 1: 013711. 10.1063/1.2838584*
31. *Lin WS, Starr TL, Harris BT, Zandinejad A, Morton D. Additive manufacturing technology (direct metal laser sintering) as a novel approach to fabricate functionally graded titanium implants: preliminary investigation of fabrication parameters. Int J Oral Maxillofac Implants. 2013; 28; 6: 1490-1495. 10.11607/jomi.3164*
32. *Traini T, Mangano C, Sammons RL, Mangano F, Macchi A, Piattelli A. Direct laser metal sintering as a new approach to fabrication of an isoelastic functionally graded material for manufacture of porous titanium dental implants. Dent Mater. 2008; 24; 11: 1525-1533. 10.1016/j.dental.2008.03.029*

33. *Cheng XY, Li SJ, Murr LE, Zhang ZB, Hao YL, Yang R, Medina F, Wicker RB. Compression deformation behavior of Ti–6Al–4V alloy with cellular structures fabricated by electron beam melting. J Mech Behav Biomed Mater. 2012; 16; Supplement C: 153-162. 10.1016/j.jmbbm.2012.10.005*
34. *Zhang X-Y, Fang G, Leeflang S, Zadpoor AA, Zhou J. Topological design, permeability and mechanical behavior of additively manufactured functionally graded porous metallic biomaterials. Acta Biomater. 2019; 84: 437-452. 10.1016/j.actbio.2018.12.013*
35. *Stanford CM. Surface modifications of dental implants. Aust Dent J. 2008; 53; Suppl 1: S26-S33. 10.1111/j.1834-7819.2008.00038.x*
36. *Ben V, Jean-Pierre K. Selective laser melting of biocompatible metals for rapid manufacturing of medical parts. Rapid Prototyp J. 2007; 13; 4: 196-203. 10.1108/13552540710776142*
37. *Yadroitsev I, Smurov I. Surface morphology in selective laser melting of metal powders. Phys Procedia. 2011; 12; Part A: 264-270. 10.1016/j.phpro.2011.03.034*
38. *Vrancken B, Thijs L, Kruth J-P, Van Humbeeck J. Heat treatment of Ti6Al4V produced by selective laser melting: microstructure and mechanical properties. J Alloys Compd. 2012; 541; Supplement C: 177-185. 10.1016/j.jallcom.2012.07.022*
39. *Shi S, Bartold PM, Miura M, Seo BM, Robey PG, Gronthos S. The efficacy of mesenchymal stem cells to regenerate and repair dental structures. Orthod Craniofac Res. 2005; 8; 3: 191-199. 10.1111/j.1601-6343.2005.00331.x*
40. *Wieding J, Jonitz A, Bader R. The effect of structural design on mechanical properties and cellular response of additive manufactured titanium scaffolds. Materials. 2012; 5; 8: 1336. 10.3390/ma5081336*
41. *Mangano C, De Rosa A, Desiderio V, d'Aquino R, Piattelli A, De Francesco F, Tirino V, Mangano F, Papaccio G. The osteoblastic differentiation of dental pulp stem cells and bone formation on different titanium surface textures. Biomaterials. 2010; 31; 13: 3543-3551. 10.1016/j.biomaterials.2010.01.056*
42. *Hindy A, Farahmand F, Tabatabaei FS. In vitro biological outcome of laser application for modification or processing of titanium dental implants. Lasers Med Sci. 2017; 32; 5: 1197-1206. 10.1007/s10103-017-2217-7*
43. *de Peppo GM, Palmquist A, Borchardt P, Lenneras M, Hyllner J, Snis A, Lausmaa J, Thomsen P, Karlsson C. Free-form-fabricated commercially pure Ti and Ti6Al4V porous scaffolds support the growth of human embryonic stem cell-derived mesodermal progenitors. Sci World J. 2012; 2012: 646417. 10.1100/2012/646417*
44. *Karageorgiou V, Kaplan D. Porosity of 3D biomaterial scaffolds and osteogenesis. Biomaterials. 2005; 26; 27: 5474-5491. 10.1016/j.biomaterials.2005.02.002*
45. *Loh QL, Choong C. Three-dimensional scaffolds for tissue engineering applications: role of porosity and pore size. Tissue Eng Part B Rev. 2013; 19; 6: 485-502. 10.1089/ten.teb.2012.0437*
46. *Sobral JM, Caridade SG, Sousa RA, Mano JF, Reis RL. Three-dimensional plotted scaffolds with controlled pore size gradients: effect of scaffold geometry on mechanical performance and cell seeding efficiency. Acta Biomater. 2011; 7; 3: 1009-1018. 10.1016/j.actbio.2010.11.003*
47. *Di Luca A, Ostrowska B, Lorenzo-Moldero I, Lepedda A, Swieszkowski W, Van Blitterswijk C, Moroni L. Gradients in pore size enhance the osteogenic differentiation of human mesenchymal stromal cells in three-dimensional scaffolds. Sci Rep. 2016; 6; 1: 22898. 10.1038/srep22898*

48. *Wu J, Mao Z, Tan H, Han L, Ren T, Gao C. Gradient biomaterials and their influences on cell migration. Interface Focus. 2012; 2; 3: 337-355. 10.1098/rsfs.2011.0124*